10/3-9-96 JSD

LBL-36877
UC-414

Lawrence Berkeley Laboratory
UNIVERSITY OF CALIFORNIA

Reduction of the Calorimeter Data with ^{208}Pb Projectiles at 158 GeV/Nucleon in the CERN Experiment NA49

I. Huang, S. Margetis, P. Seyboth, and D. Vranic

December 1995

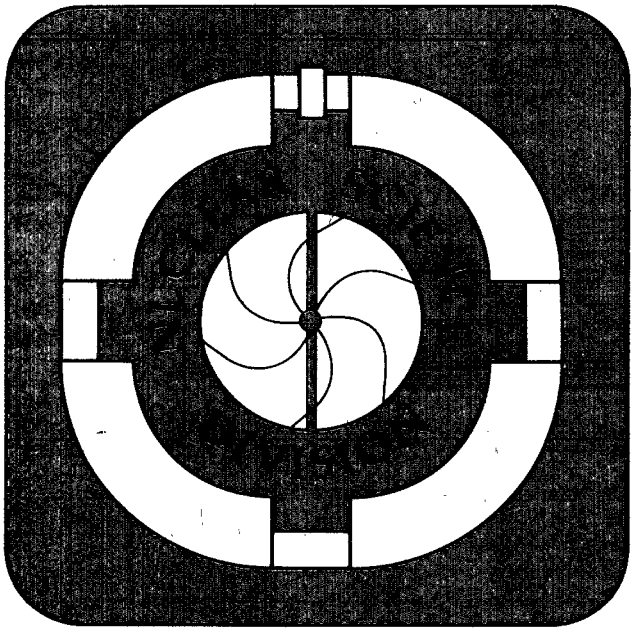

Prepared for the U.S. Department of Energy under Contract Number DE-AC03-76SF00098

DISCLAIMER

Available to DOE and DOE Contractors
from the Office of Scientific and Technical Information
P.O. Box 62, Oak Ridge, TN 37831
Prices available from (615) 576-8401

Available to the public from the
National Technical Information Service
U.S. Department of Commerce
5285 Port Royal Road, Springfield, VA 22161

Ernest Orlando Lawrence Berkeley National Laboratory
is an equal opportunity employer.

LBL-36877
UC-414

Reduction of the Calorimeter Data with 208Pb Projectiles at 158 GeV/Nucleon in the CERN Experiment NA49

I. Huang, S. Margetis, P. Seyboth, D. Vranic
Lawrence Berkeley Laboratory
University of California, Berkeley, CA 94720

December 1995

This work was supported by the Director, Office of Energy Research, Division of Nuclear Physics of the Office of High Energy and Nuclear Physics of the U.S. Department of Energy under Contract DE-AC03-76SF00098

 35

LBL–36877
UC–414
December 1995

Reduction of the Calorimeter Data with ^{208}Pb Projectiles at 158 GeV/Nucleon in the CERN Experiment NA49

I. Huang[1], S. Margetis[2], P. Seyboth[3], D. Vranic[4]

[1] *University of California, Davis, CA 95616 USA*
[2] *Lawrence Berkeley Laboratory, Univ. of California, Berkeley, CA 94720 USA*
[3] *Max Plank Institut für Physik, Munich, Germany*
[4] *Gesellschaft für Schwerionenforschung (GSI), Darmstadt, Germany*

ABSTRACT

The first heavy ion run involving a ^{208}Pb beam at E_{LAB}=158 GeV/Nucleon was performed at the CERN Super Proton Synchrotron (SPS) in November–December 1994. The calibration procedures and the analysis of the calorimeter data are presented.

1. NA49 Calorimeters

The NA49 calorimeter setup is shown in Fig. 1. The beam is defined by a 0.2 mm quartz Cherenkov counter followed by a veto scintillator counter with a 10 mm central hole. Another veto scintillator paddle counter (S_5) was placed just below the beam 4.4 meters upstream of the calorimeter target in order to suppress non-target interactions (see below). There are two calorimeters, the mid-rapidity (Ring) calorimeter ($2.1 < \eta < 3.4$) and a beam (Veto) calorimeter. Both detectors have been previously used in NA5, NA24 and NA35.[1,2] The Ring calorimeter is tube-shaped with an inner radius of 28 cm and outer radius of 149 cm. It has two parts, a 16 radiation lengths (X_0) photon (or electromagnetic) part in front followed by a hadron part of 6 interaction lengths (λ_{int}). Since the thickness of the photon part is 1 λ_{int} this gives a total of 7 λ_{int}. Each part is divided into 24 azimuthal sectors and 10 radial rings thus resulting in a total of 240 cells for each part. The radial cell size varies so that the cells in a sector cover pseudo-rapidity intervals of equal size.

The Veto calorimeter is likewise divided into a photon part and a hadron part.[1] It was originally constructed with four cells with a center hole. However, in NA49 the hole was closed up and the four scintillator sheets were glued together. The acceptance of the Veto calorimeter is defined by the aperture of an iron collimator, 11 meters from the target, with an opening of 10x10 cm^2 at the front and 10x12.4 cm^2 at the back end. This corresponds to about 0.3 degrees around the beam axis in the lab frame (or 5.0 degrees in the center-of-mass frame) and it mainly covers the projectile spectator region for most impact parameters.

Two target positions were used during the data taking (Fig. 1). The nominal target (2% λ_{int}^{Pb}) is positioned (Target 1) 6 meters upstream from the face of the Ring Calorimeter (which then covers the kinematic region around mid-rapidity). Another position (Target 2) 10.4 meters upstream was used mainly for calibration purposes (see below). Two types of triggers were used. In order to preserve the effective E_T of each particle the NA49 magnets were turned off for the calorimeter runs.

2. Calibration procedure and response simulations

The behavior of the calorimeters has been studied in the past.[1,2] In NA49, however, the GEANT simulation package was used as an extra tool in understanding the response of the Ring calorimeter. There are several correction factors applied to the raw data in the analysis chain, and GEANT served as an independent check in most cases. Fig. 2 describes the calibration and analysis procedure of the

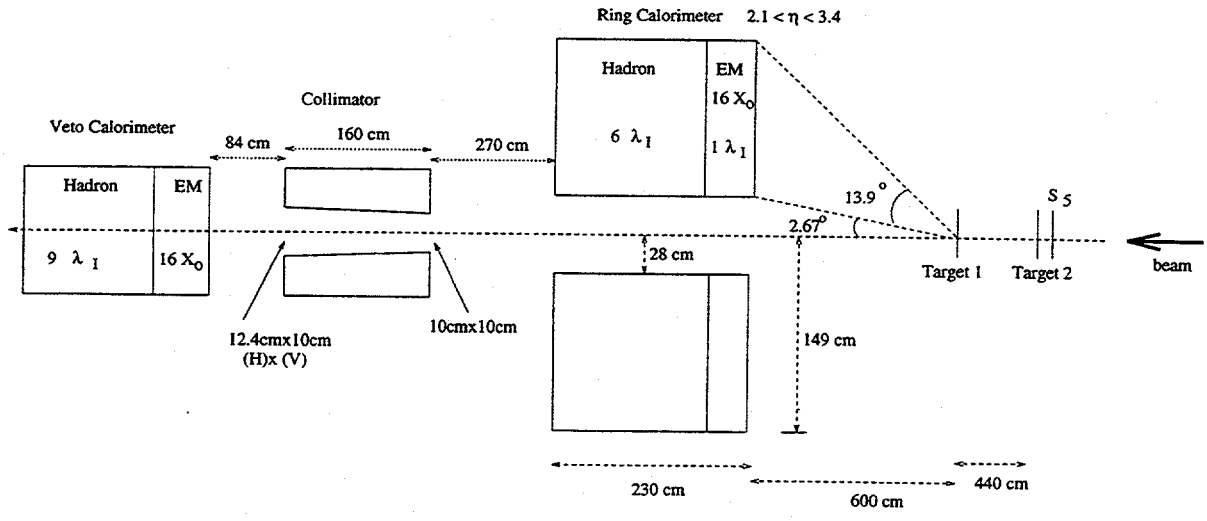

Fig. 1. Top view of the structure of the NA49 Calorimeters.

Ring calorimeter data. After a series of corrections specific to the electronics and the construction of the Ring calorimeter, the analysis chain splits into two branches: (1) the 'NA35' chain which is the traditional NA35 analysis chain adapted to theNA49 environment, and (2) the alternative in which corrections were derived exclusively from GEANT simulations. The main difference between the two is that in the 'NA35' chain there is a separate correction factor for each individual effect (see below), but in the 'GEANT' chain there is basically a single cell–response factor which corrects for several individual effects (with the only exception of cell non–uniformity). The following items are dealt with in the analysis chain (The items in parentheses are indicating the method(s)/tool(s) used to evaluate the corresponding correction factor):

- Gain reduction and calibration of the Ring calorimeter (Calibration beams, GEANT)
- Optical cross talk (Data)
- Calibration factors for hadrons and electrons
- Determination of e/π ratio (Data, GEANT)
- Mean energy deposited by hadrons in the photon part (Data+Monte Carlo(MC), GEANT)
- Correction for inclined incidence and lateral shower containment(MC, GEANT)
- Non-uniformity factors & nonlinear response to low energy hadrons (Data, Old Data+MC, GEANT)
- Veto calorimeter calibration and acceptance simulation (Data, MC, GEANT)

2.1. Gain reduction

Since the amount of transverse energy released in a Pb+Pb collision is much more than that in a S+Au collision, we had to reduce the gains of the photomultipliers of the six inner rings of the Ring calorimeter in order to avoid exceeding the ADC dynamic range. The gains are reduced by lowering the high voltage (HV) of the photomultiplier tubes (PMT) according to the formula:

$$n = \left(\frac{HV_{old}}{HV_{new}}\right)^{g} \qquad (1)$$

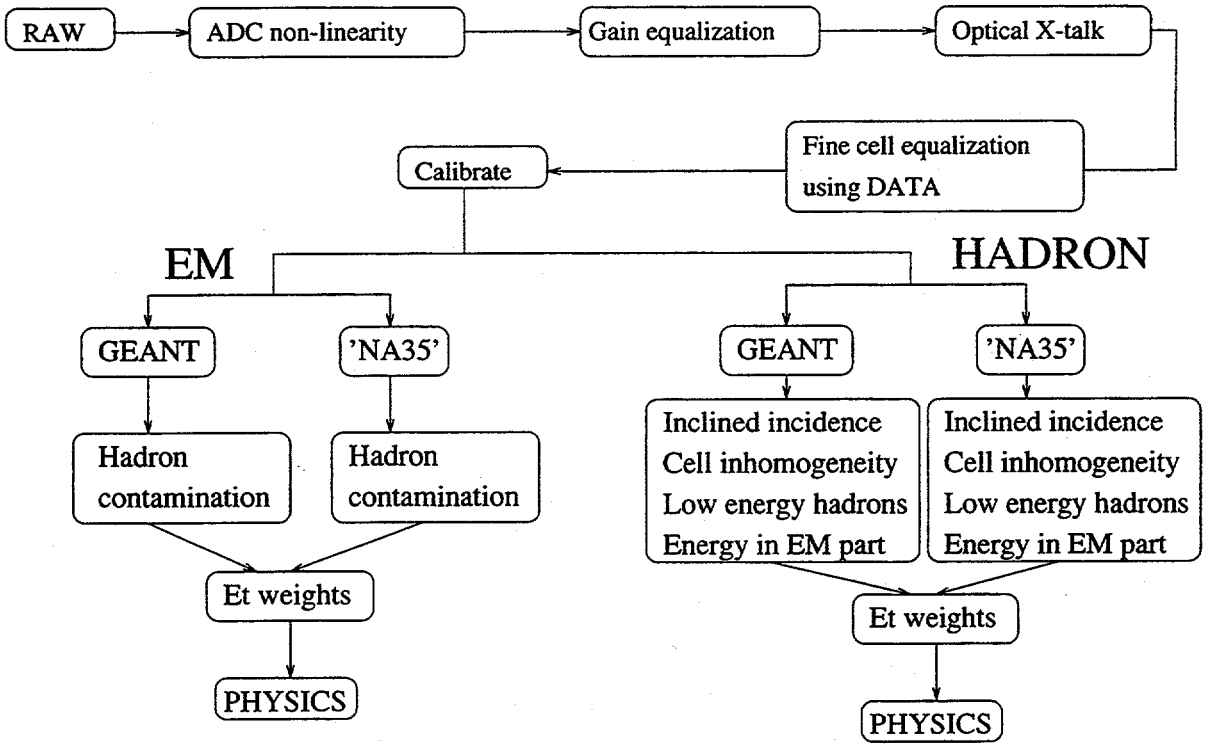

Fig. 2. Flow chart of the calibration and analysis of the Ring Calorimeter data. Although the names of the correction factors are the same for both chains, the actual method of estimation was different.

where n is the reduction factor and g is the gain exponential (≈ 8.0) particular to each cell, obtained from previous studies. The initial calculations suggested the gain reduction factors listed in Table 1 in relation to the NA35 configuration. However, during the initial phase of the lead run, we noticed

Ring number	1	2	3	4	5	6	7	8	9	10
Photon part	3.0	3.0	2.5	2.0	1.5	1.5	1.0	1.0	1.0	1.0
Hadron part	3.0	2.0	2.0	2.0	1.5	1.5	1.0	1.0	1.0	1.0

Table 1. Factors by which the gain of each ring was reduced from the NA35 settings.

that ring 1 registered much more energy than anticipated. The reason is that some particles can penetrate into the first ring from the inner surface of the hole, not just the front face*. The gain in the first ring was readjusted, but the attempt to estimate proper correction factors for the innermost ring was not successful. This is mainly due to the complicated and convoluted way the signal in that ring was formed (e.g. electromagnetic energy directly seen in the hadron part, partial shower development/containment for particles hitting the calorimeter close to the back, etc.). In the end, we decided to ignore the signals from the first two rings, considering them as a shield for the rest of the rings. This reduced the Ring calorimeter acceptance to $2.10 < \eta < 3.43$ for the 6 meter target position.

2.2. Optical cross talk & ADC nonlinearity

There is some optical cross talk between the photon and hadron part because of the common readout system used in the Ring calorimeter. The results from a study done in NA35[2] were used to correct for the effect. Also, a similar NA35 study measured the nonlinear behavior of the used ADCs. The same correction factors were applied to the raw data also in NA49.

2.3. Calibration of the Ring calorimeter for single hadrons and electrons

Shortly before the lead run, a calibration run was performed, which employed 30 GeV electron and pion beams – for the photon and hadron sections respectively. The calorimeter was rotated and translated such that the beams were directly incident on a predetermined calibration point of a cell. The ADC values of a cluster of neighboring cells around the calibration cell were summed. We define $E_{HAD} = GEVHAD \cdot ADC_{HAD}$ and $E_{EM} = GEVGAM \cdot ADC_{PHOTON}$. For electrons, the cluster ADC distribution was a nice gaussian distribution (Fig. 3), and therefore the extraction of the calibration constant GEVGAM was a straight-forward matter. There is a small shower leakage out of the EM part to the hadron part (estimated to be about 5%). However, this effect is self-correcting because in the processes of both calibration and data analysis we assumed full shower containment.

For hadrons, however, cuts in the correlation between ADC_{had} and ADC_{photon} were made in order to eliminate: (1) muon signals (from pions decays), and (2) showers starting in the EM part (Fig. 4). The projected ADC distribution onto the ADC_{had} axis, after the cuts, was fitted with a Gaussian, and its peak was used for calibration (GEVHAD). In a multiparticle environment where individual showers are not reconstructed one should calibrate with the mean, not the most probable (peak) response. This was done for the GEANT chain. However, one of the correction factors in the 'NA35' chain explicitly takes care of the difference between the mean and the peak calibration (see NA5 non-uniformity correction below) and therefore we kept the traditional 'peak' calibration method in the 'NA35' chain. The measured ratio between mean and peak calibration constants was compared with the one from NA5/NA35 and found to be identical, which shows that the 'global' behaviour of the calorimeter is stable in time.

In order to have a unique calibration constant for all cells, a reference cell was chosen and relative calibration factors were calculated for all the rest. The whole procedure was iterated several times since showers spread over several cells and the calibration of a cell affects the overall calibration of its neighbors.

*In NA35 this was not the case because of the presence of the intermediate calorimeter.

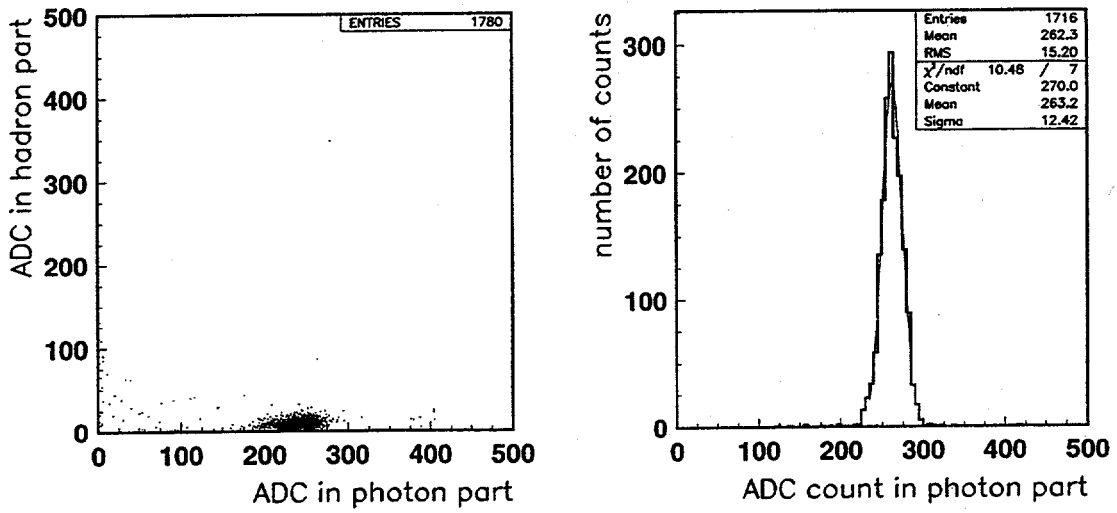

Fig. 3. Correlation plot of the ADC counts in the hadron vs. the photon part for a 30 GeV electron beam incident on cell 67 (left), and its projection onto the photon axis. The solid line is a gaussian fit to the data.

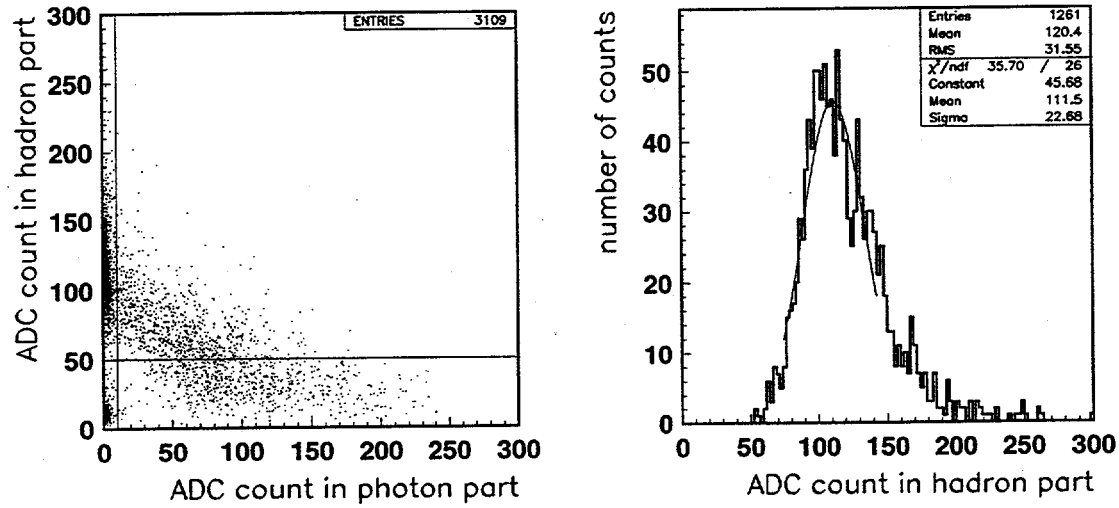

Fig. 4. Correlation between the cluster ADC counts in the hadron vs. the photon part for a 30 GeV pion incident beam (left). The cut lines show the selected region (upper left slice) which consists of showers starting in the hadron part ($E_{EM} \approx 0$), and are free of muons (blob at the axes origin). The projection of this particular area projected onto the hadron axis is shown on the right histogram. The solid line is a gaussian fit to the peak.

A total of three sectors, i.e. 30 cells were calibrated. The rest were tuned when the lead beam became available. Then, we illuminated all the cells of the Ring calorimeter with particles from central Pb+Pb collisions, and assuming symmetric distribution of energy in azimuth on average, we calculated correction factors which equalized the response of the un-tuned cells with the average response of the calibrated cells in the same ring.

From the widths of the distributions in fig. 3,4 we calculated the energy resolutions of individual showers at different radial positions. They are $\sigma(E)/E = 20 - 40\%/\sqrt{E}$ (GeV) for the photon section and $\sigma(E)/E = 100 - 140\%/\sqrt{E}$ (GeV) for the hadron section. They tend to get worse towards the inner cells which have smaller cell sizes, i.e. less shower containment.

2.4. The e/π ratio of the EM part

Particles that induce electromagnetic showers in a calorimeter give, in general, a different (higher) response from those that induce hadronic showers. This is because in a hadronic shower some amount of the initial energy is spent in breaking up the target nucleus (nuclear binding effect). Therefore, the amount of energy deposited by hadrons in the photon part must be multiplied by the e/π ratio in order to be correctly calibrated. The e/π ratio can be obtained from the correlation plot of E_{TOT} versus E_{EM} for incident hadrons. E_{TOT} is the sum of the energy deposited in each part of the calorimeter: $E_{TOT} = E_{HAD} + (e/\pi) * E_{EM}$. If the correct e/π factor is used the resulting E_{TOT} distribution should be clustered around the incident hadron energy. This factor was found to be 1.4 (see Fig. 5) at 30 GeV. This value, which was confirmed by GEANT (Fig. 5), is a typical value for a Pb/Scint. sampling calorimeter.

2.5. Hadronic energy in the photon part

The photon part is one interaction length long, and thus part of its signal is due to hadron showers. We estimated the fraction of hadronic energy in the photon part using GEANT. The results are shown in Fig. 7. The GEANT 30 GeV result was found to be in close agreement with the calibration data obtained with 30-GeV pions. The results at different energies were then fitted by the function:

$$f(E)[\%] = 23.5 + \frac{41.7}{E[GeV]} \tag{2}$$

The fit function was then used together with VENUS central Pb+Pb events to estimate the (average) fraction of hadronic energy in the photon part of each ring. The overall result is that about 50% of the signal in the EM part is of hadronic origin. The estimated factors were then used during the analysis in order to calculate the energy due to photons and hadrons in the EM part of the calorimeter.

2.6. Correction for inclined incidence and lateral shower containment

Particles fly into the cylindrical Ring calorimeter at various angles, and since the rings do not have a projective geometry, showers (especially hadron showers) traverse multiple rings. Since each ring is weighted differently (in order to estimate E_T from the energy deposition), the overall effect is an overestimation of the true E_T. Although this effect is implicitly corrected in the GEANT chain of analysis, we wanted to have an estimation of it for the 'NA35' chain. In order to do this outside GEANT one needs a parametrization of the transverse as well as the longitudinal profile of the hadronic shower. We parametrized the transverse profile of hadronic showers using test run data with 30 GeV particles. We then distributed the initial energy at five different equidistant points

Ring number	3	4	5	6	7	8	9	10
E_{true}/E_{seen}	0.909	0.854	0.853	0.850	0.813	0.805	0.790	0.869

Table 2. Monte Carlo estimation, using VENUS and longitudinal and transverse shower parametrizations, of the shower spreading combined with the inclined incidence effect.

separated by 40 cm(see Fig. 8). The weighting factors for the energy distribution at these five points

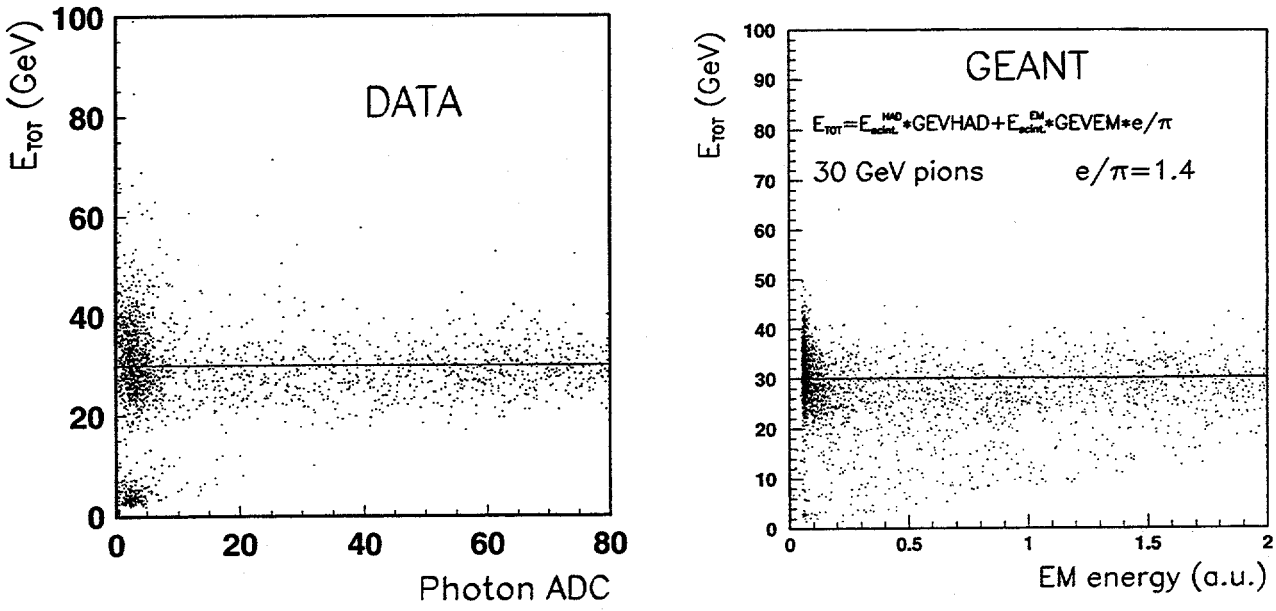

Fig. 5. Total energy (E_{TOT}) in the Ring calorimeter, with the e/π ratio of the EM part folded in, for 30 GeV pions. The E_{TOT} as a function of E_{EM} for calibration data (left) is compared to a GEANT simulation (right). In both cases $e/\pi = 1.4$.

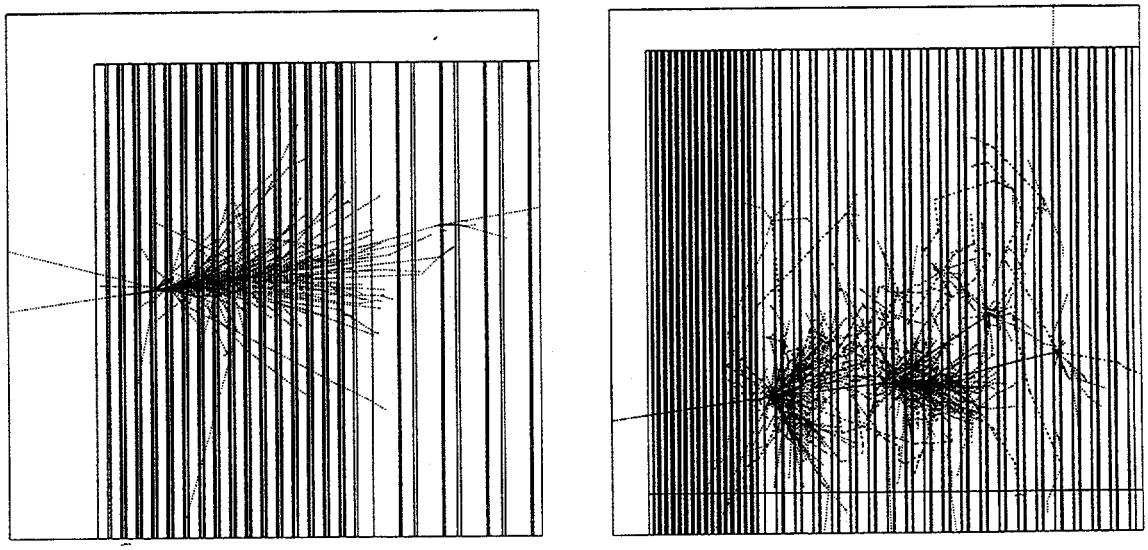

Fig. 6. Pictures of GEANT-simulated showers created by a 4 GeV gamma ray in the EM part (left) and a 30 GeV pion in the hadron part (right) of the Ring calorimeter.

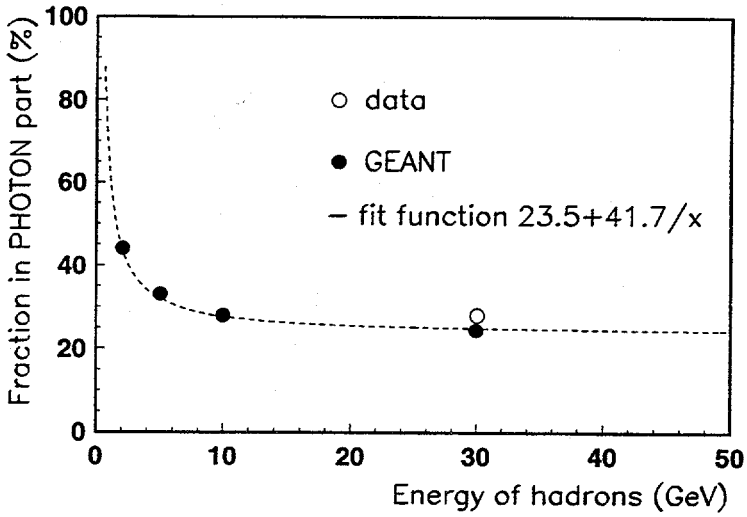

Fig. 7. GEANT estimation of the fraction of hadronic energy deposited in the photon part (filled circles). The corresponding point from the calibration data at 30 GeV is also shown (open circle).

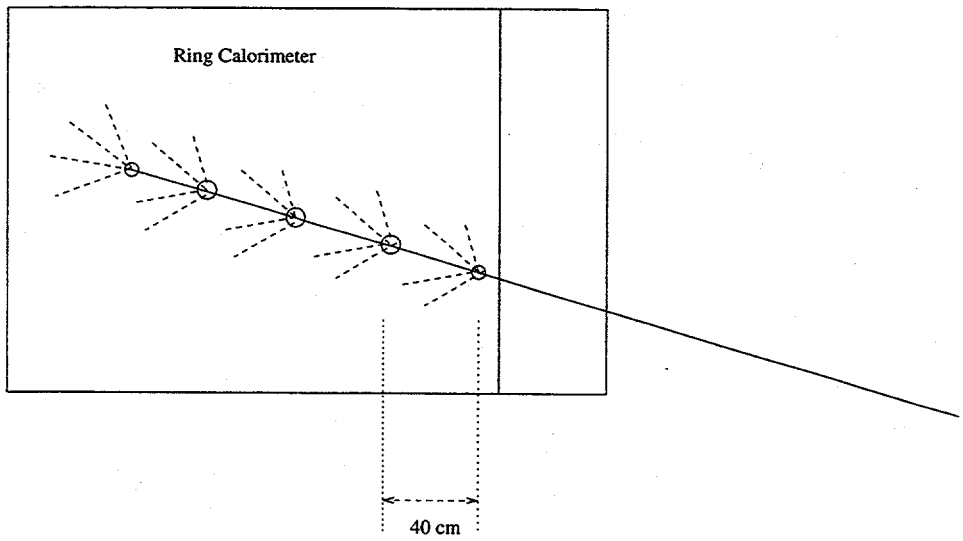

Fig. 8. Simulation of an inclined hadron shower by a series of five showers with the parametrization obtained from data.

were obtained from GEANT longitudinal shower profiles at different energies. One thousand VENUS central Pb+Pb events were then processed, and the resulting correction factors are summarized in Table 2. Depending on the ring position the effect has a magnitude of 10–20%. It is in good agreement with results obtained from GEANT calculations with full shower simulation in which the inclined incidence of showers is implicitly built in.

2.7. Nonuniformity factors & nonlinear response to low energy hadrons

Each cell of the Ring calorimeter has a non-uniform response, i.e. the output signal depends on the location of the hit. The reason for this effect was identified to be the presence of the acrylic readout rods which act as 'hot spots' (particles produce UV light as they traverse them). The calibration was done at a particular position for each cell, where the response is about the average response of the cell. During data-taking, particles are distributed rather uniformly across a cell and it is difficult, in general, to check shifts in the calibration due to non-uniformities.

Another effect is that low energy hadrons ($< 3\,\mathrm{GeV}$) give in general a higher response. In NA5, a parametrization of prototype measurements resulted in the estimation of the cell response as a function of incident energy and ring number. This is shown in Fig. 9 which shows the ratio of the average cell response to the most probable value (which was found to be proportional to the incident particle energy), for particles uniformly distributed over the cell surface. We see that the response gets higher as the incident energy gets lower. In the same figure and for a given energy, the difference between any two rings is due to different non-uniformity factors. Notice that ring 7 exhibits the strongest non-uniformity which correlates with the fact that it is the innermost ring with two readout rods, thus having the largest ratio of 'hot spot'/total area. These measurements together with VENUS events were put in a Monte Carlo simulation and an initial set of correction factors was obtained. The GEANT simulation did not have the non-uniformity effect built in, but the response to low energy hadrons was assumed to be implicitly in.

In order to check the inter-ring calibration and estimate at the same time any residual non-uniformity effects, we compared data taken with the target placed in two different positions. Since a given pseudo-rapidity region is seen by different rings at different target positions, the behavior of the data in the common acceptance could be used to check for any residual effects. Figure 10 (left histogram) shows, as an example, the 'raw' pseudo-rapidity distribution of the Hadron energy for both upstream and downstream (nominal) target positions. Only central events were selected, and since the Veto acceptance varies with the target position, in order to avoid any trigger differences the selection of the events was done off-line using the corresponding $E_T - E_{VETO}$ correlation plots. We see that ring 7 is systematically higher than the rest. By fitting each distribution with a gaussian function (with the mean value fixed at $\eta = y_{cm}$), an average set of non-uniformity correction factors can be estimated for each part of the detector. The resulting factors are summarized in Table 3. The factors are different between the GEANT chain (which did not have any correction applied) and the 'NA35' chain which had already some non-uniformity correction in the NA5 factors. The overall effect is small.

Ring number	3	4	5	6	7	8	9	10
GEANT chain								
EM part	0.96	1.01	1.01	1.00	0.90	1.02	1.07	0.95
HADRON part	0.85	0.85	1.00	1.25	0.92	1.05	1.00	0.90
'NA35' chain								
EM part	1.00	1.00	1.00	0.98	0.92	1.02	1.00	0.96
HADRON part	0.90	0.95	1.00	1.12	0.95	1.05	1.05	0.90

Table 3. Non-uniformity correction factors for each part of the calorimeter and for each analysis chain.

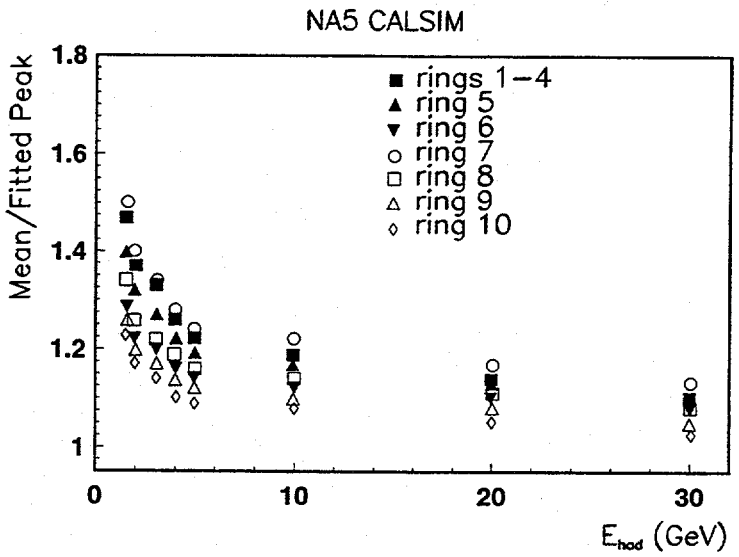

Fig. 9. Ring average response, relative to the incident beam energy (see text), as a function of incident hadron energy based on NA5 measurements, for different rings.

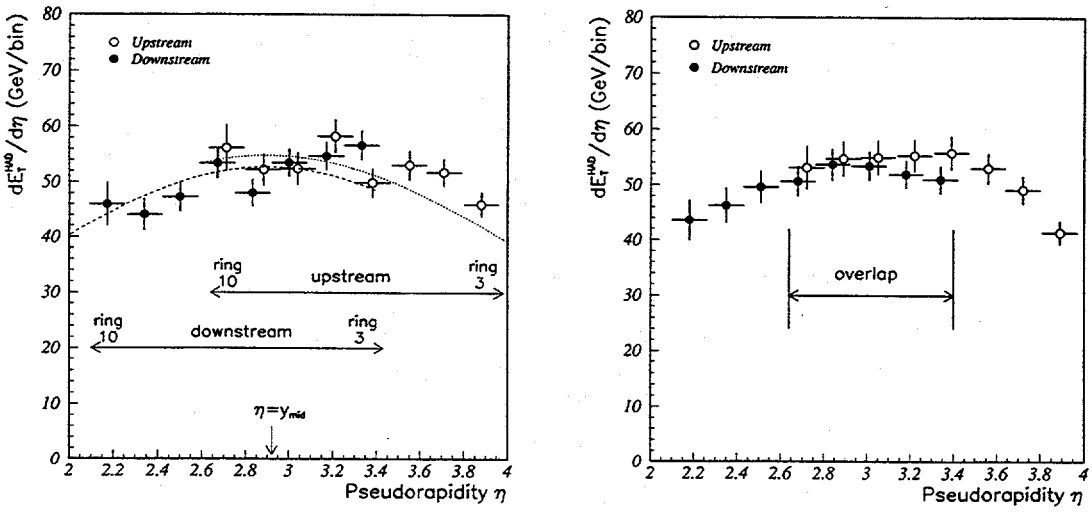

Fig. 10. $dE_T^{HAD}/d\eta$ distribution before (left) and after (right) the non-uniformity correction for both up/downstream data.

2.8. Veto Calorimeter

The Veto calorimeter was first calibrated with hadrons and at the same time the voltages on the four photomultipliers in each section (reading the common cell) were adjusted so that all four were giving about the same signal for an incident beam at the center of the detector. During data taking the calibration constant was normalized to the Pb beam energy (about 33 TeV). The calibration was then checked for each individual run. We found that it slightly shifted ($< 5\%$) two times over the calorimeter data taking period. The energy seen by the Veto calorimeter is mainly hadronic, even for head-on collisions the hadronic component is more than 10 times the electromagnetic one. Therefore the Veto was calibrated as a hadron calorimeter and the energy was calculated according to the following formula:$E_{VETO} = (ADC_{PHOTON} * e/\pi + ADC_{HADRON}) * GEVVETO$, where GEVVETO is the calibration constant and $e/\pi = 1.4$.

In order to compare with model predictions the Veto acceptance should be known to high accuracy. Part of the showers induced near the end of the hole of the collimator are 'leaking' to the Veto calorimeter, and this could lead to an underestimation of the true acceptance. We performed a GEANT simulation of the Veto response using central VENUS Pb+Pb events, and we compared that to simple calculations where a sharp cut acceptance of the collimator hole was used. The average difference between the two was 2.5%, which we consider negligible.

3. Data analysis

3.1. Non-target interactions

Each data taking run was followed by a run without a target in order to allow for background subtraction. The background consists of non-target interactions, mainly beam-gas interactions. After proper normalization the target-out cross-section was subtracted from the corresponding target-in run. The background interactions mainly populate the relatively low E_T region (Figs 11, 12), where they are up to 10 times larger than the real signal. Unfortunately, the data in this low E_T region were taken with a relatively thick Pb target (3 mm), and both rescattering of the produced particles and interactions of spectator fragments in the target are not negligible. Rescattering has always the tendency to increase the effective E_T, i.e. cross section from the very low E_T region shifts toward higher E_T values. This can be seen in Fig 13 where in the region 50–150 GeV the data is systematically higher than model predictions. A study was performed with GEANT which confirmed qualitatively the above hypothesis. However, due to the complexity of the situation, a reliable correction procedure could not be derived.

3.2. GEANT - 'NA35' chain comparison

In figures 14,15 we make a comparison between the results from the GEANT and the 'NA35' chain. The comparison of the total E_T is presented in Fig. 14 for a medium bias run. We see that the difference between the two chains is at the percent level. In Fig. 15 (top two histograms) we make the comparison at the individual E_T^{EM} and E_T^{HAD} level. The two bottom histograms are the ratio E_T^{EM}/E_T^{HAD}. We consider the difference as being insignificant. We also compared the results of the two chains as a function of ring number, but no systematic differences were found We used the difference between the two chains to estimate our systematic uncertainty.

3.3. EM/HAD ratio

The ratio E_T^{EM}/E_T^{HAD} is a very delicate but, at the same time, very important physics quantity. This is because anomalous fluctuations in the production of these two quantities can signal a possible phase transition[†] and also because the hadron contamination in the EM part might smear any original effect. Using VENUS and GEANT we tried to get a feeling for the sensitivity of our detector to such fluctuations, and at the same time understand the results.

There are two features in this ratio that are important: the mean and the width. The first one, the mean value, is of particular interest for central events. It is obvious that a large departure of the mean value from model predictions will signal interesting physics. Experimentally though, any

[†] E_T and Energy are closely correlated in relatively small acceptance, according to simulations.

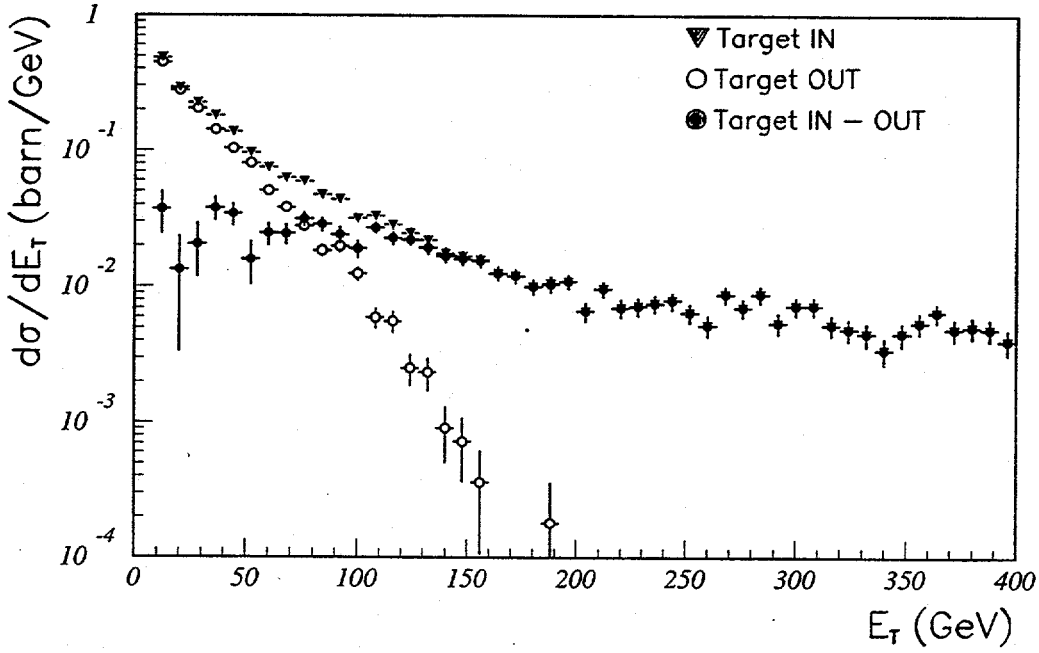

Fig. 11. Determination of the transverse energy cross section. The target-in, target-out normalized cross section and the difference are shown.

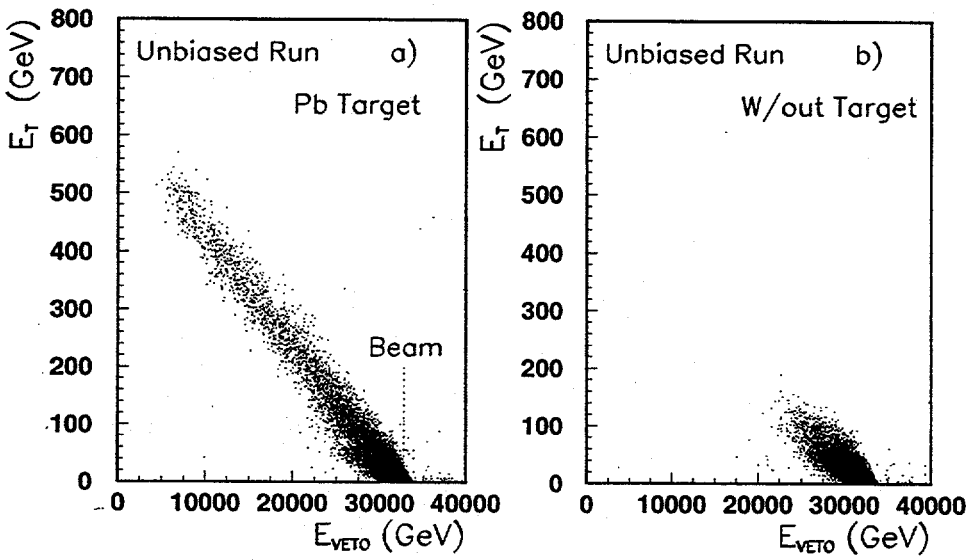

Fig. 12. Correlation between E_T and E_{VETO} for target-in (left) and target-out (right) runs.

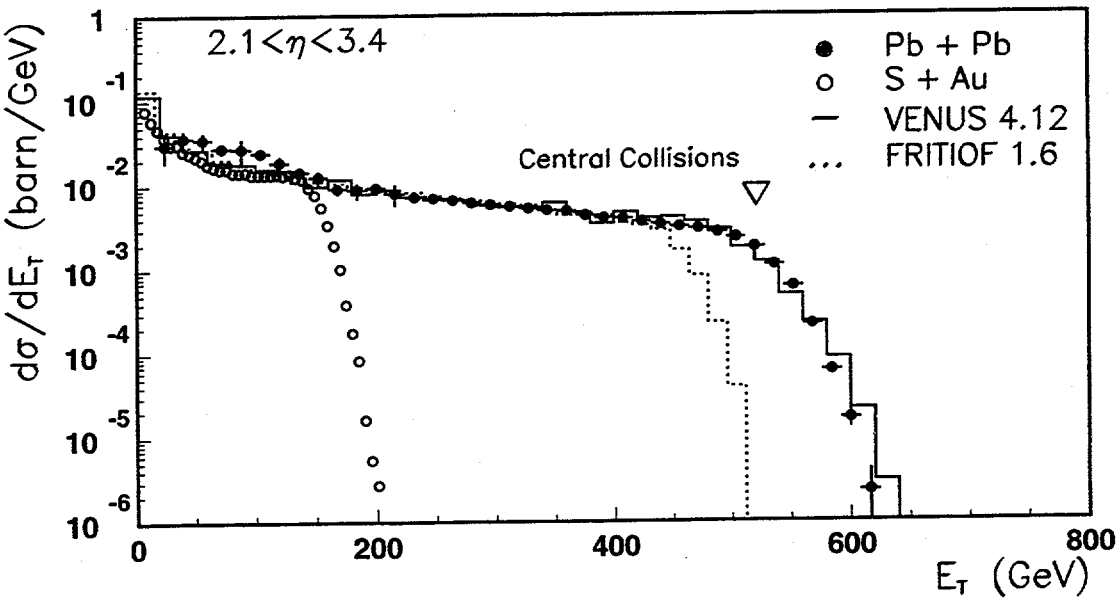

Fig. 13. Transverse energy spectrum for Pb+Pb collisions at 158 GeV/A.

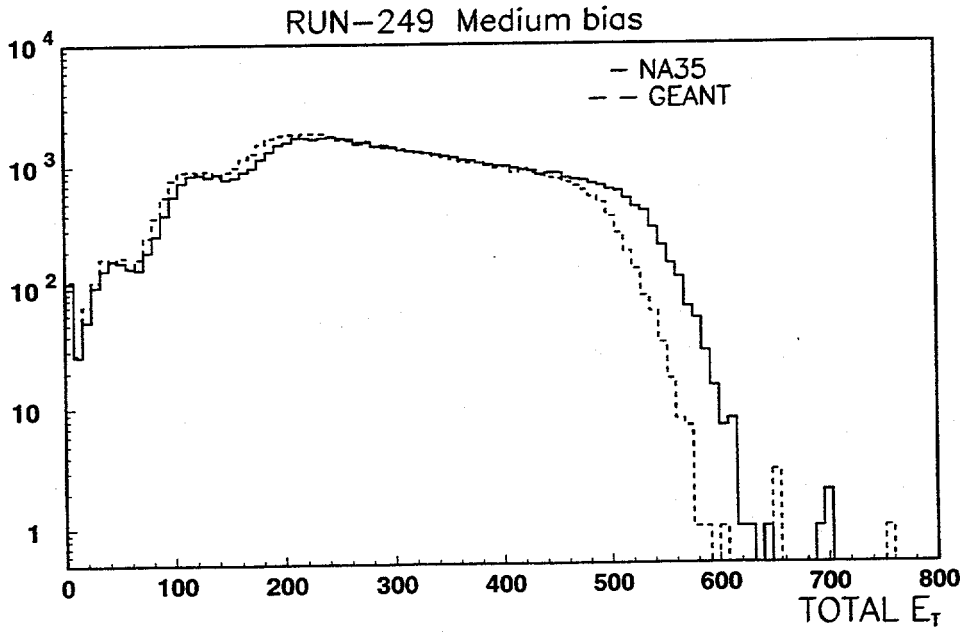

Fig. 14. Transverse energy distribution compared for the GEANT and 'NA35' correction chains.

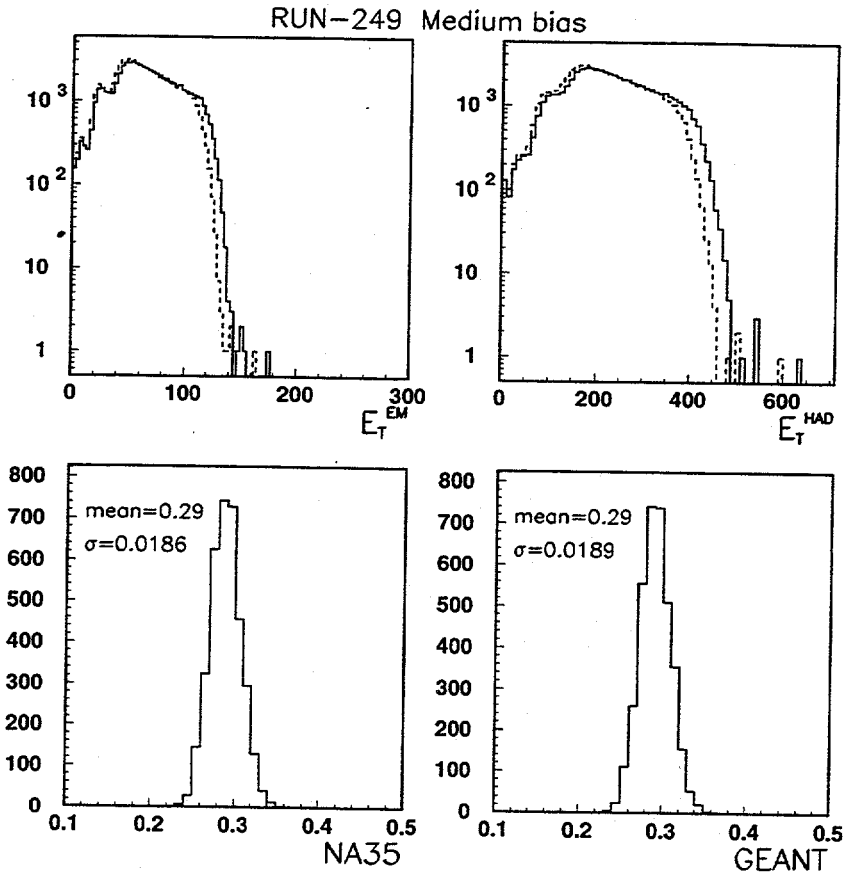

Fig. 15. Comparison of GEANT (dashed line) and 'NA35' chain (solid line) for E_T^{EM} (upper left), E_T^{HAD} (upper right). The lower histograms are the resulting ratios E_T^{EM}/E_T^{HAD} for a sample of central collisions.

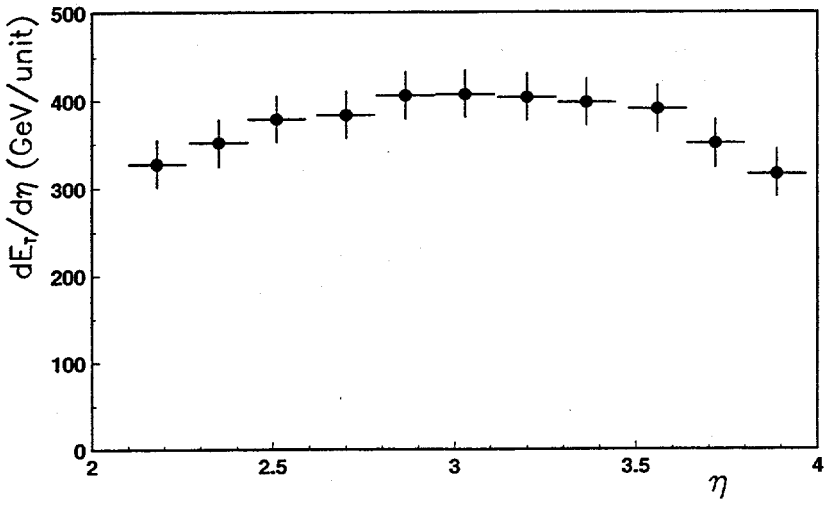

Fig. 16. Normalized $dE_T/d\eta$ distribution. The errors are only systematic and their values are the average difference between results from the two correction chains.

miscalculation of the E_T^{EM} during the unfolding procedure will immediately be reflected in the mean value of the ratio. Therefore the mean value has large systematic errors of about 10–15%.

The width of the E_T^{EM}/E_T^{HAD} distribution is in principle immune to shifts of the mean value. Actually, the observed width is a convolution of the following effects:

- **Intrinsic (natural) width.** This is a combination of fluctuation due to the finite detector acceptance, and fluctuations in particle composition of the event at the collision level.
- **Sampling fluctuations.** This is purely instrumental.
- **'Mixing' (coupling) fluctuations.** This is due to the unavoidable fact that hadron energy is contaminating the EM signal, and also due to the associated correction methods (see below).

Looking at the intrinsic width in VENUS events, we found that EM fluctuations are twice as large as the fluctuations of hadronic energy, thus dominating the width of the ratio. Also, GEANT simulations showed that sampling fluctuations are significantly smaller than the intrinsic ones, thus having only a minor effect on the combined width. This suggest that the sensitivity of the detector is adequate. The last factor, the mixing fluctuations, is more complicated. It is basically the fact that part of the denominator in the ratio enters the numerator thus weakening the overall effect. On top of this, the specific unfolding procedure of the EM signal can further complicate matters. Simulations showed that the most 'innocent' procedure would be the one where a correction factor is directly applied to the EM signal in order to extract the EM energy. This is the method which was adopted during the analysis, e.g. E_{EM}=(calibrated signal)x(correction factor[≈50%]). The same way we obtained E_{HAD}.

3.4. $dE_T/d\eta$

The $dE_T^{TOT}/d\eta$ distribution after the non-uniformity correction, for central Pb+Pb collisions is shown in Fig. 16. The data points in this histogram are the average between the two analysis chains, and the errors are the average difference between them, therefore the errors are systematic only. One of the advantages of this extented acceptance is that the extrapolation factor to 4π is reduced (from 2.5 to 1.9), which also reduces the dependence on the event generator used for determining this factor.

3.5. Number of binary collisions

We cite here the analytical formulas used in the calculation of the number of collisions a participant suffers in various collision systems. In the case of Pb+Pb (i.e. symmetric) collisions, this number is given by the formula[2]

$$< \nu >= \frac{3r_0}{2\lambda_{inel}} A^{\frac{4}{3}} \tag{3}$$

where r_0=1.16 fm and λ_{inel} is the mean free path for inelastic NN collision. Using the inelastic pp cross section σ_{inel}^{pp} = 33 mb, we get

$$\lambda_{inel} = \frac{1}{\rho_0 \sigma_{inel}^{pp}} = \frac{4\pi r_0^3}{3\sigma_{inel}^{pp}} = 2.0 fm \tag{4}$$

$$< \nu >= 1072\ (88) \tag{5}$$

for Pb+Pb (S+S).

For an asymmetric collision (e.g. S+Au), the formula is more complicated[2]:

$$< \nu >= \frac{\pi \rho_0}{\lambda_{inel}} r_0^4 [(A^{2/3} + B^{2/3}) A^{1/3} B^{1/3} + \frac{1}{2}(B^{2/3} - A^{2/3})^2 ln(\frac{B^{1/3} - A^{1/3}}{B^{1/3} + A^{1/3}})] \tag{6}$$

where $\rho_0 = 1/(\frac{4\pi r_0^3}{3})$, A is the projectile and B the target mass. For S+Au, $< \nu >$ is 202.3.

4. Summary

- Because of the large amount of energy seen by the calorimeter in the Pb+Pb collisions, the gains of the inner six rings of the Ring Calorimeter were reduced from the NA35 settings. The inner two rings were disregarded due to large contributions from particles that went directly into the inner surface of the hole.
- The calibrations of the Calorimeters were done with 30-GeV electron and pion beams. The energy resolutions were found to be about $30\%/\sqrt{E(GeV)}$ for the photon part and $100\%/\sqrt{E(GeV)}$ for the hardon part. The e/π response ratio was 1.4.
- The optical cross-talk effect and ADC nonlinearity were corrected for in the analysis.
- The separate energy contributions of photons (from π^0, η etc. decays) and of hadrons were derived.
- The effect of inclined particle incidence on the determination of E_T was taken into account.
- Results on $d\sigma/dE_T$, $dE_T/d\eta$ and E_T^{EM}/E_T^{HAD} were obtained. The measured and corrected E_T spectrum favors the predictions of VENUS over FRITIOF.

5. ACKNOWLEDGMENTS

The authors would like to thank Dr. Thomas Wienold for his contribution in taking and interpreting data. This work was supported in part by the Director, Office of Energy Research, Division of Nuclear Physics of the Office of High Energy and Nuclear Physics of the U.S. Department of Energy under contract DE-AC03-76SF00098.

References

1. C. de Marzo et al.; NIM 217 (1983) 405
2. J. Bächler et al.; Z. Phys. C52(1991)239
   S. Margetis; Ph.D. Thesis, Frankfurt 1990, GSI report, 91-04